

---

# KHRONOS: a Kernel-Based Neural Architecture for Rapid, Resource-Efficient Scientific Computation

---

**Reza T. Batley**

Kevin T. Crofton Department of Aerospace and Ocean Engineering  
Virginia Polytechnic Institute and State University  
Blacksburg, VA 24060  
rezabatley@vt.edu

**Sourav Saha**

Kevin T. Crofton Department of Aerospace and Ocean Engineering  
Virginia Polytechnic Institute and State University  
Blacksburg, VA 24060  
souravsaha@vt.edu

## Abstract

Contemporary models of high-dimensional physical systems are constrained by the curse of dimensionality and a reliance on dense data. We introduce KHRONOS (Kernel-Expansion Hierarchy for Reduced-Order, Neural-Optimized Surrogates), an AI framework for model-based, model-free and model-inversion tasks. KHRONOS constructs continuously differentiable target fields with a hierarchical composition of per-dimension kernel expansions, which are tensorized into modes and then superposed. We evaluate KHRONOS on a canonical 2D, Poisson equation benchmark: across 16-512 degrees of freedom (DoFs), it obtained  $L_2^2$  errors of  $5 \times 10^{-4}$  down to  $6 \times 10^{-10}$ . This represents a  $\sim 100\times$  gain over Kolmogorov-Arnold Networks (which itself reports a  $\sim 100\times$  improvement on MLPs/PINNs with  $100\times$  fewer parameters) when controlling for the number of parameters. This also represents a  $\sim 10^4\times$  improvement in  $L_2^2$  error compared to standard linear FEM at comparable DoFs. Inference complexity is dominated by inner products, yielding sub-millisecond full-field predictions that scale to an arbitrary resolution. For inverse problems, KHRONOS facilitates rapid, iterative level set recovery in only a few forward evaluations, with sub-microsecond per-sample latency. KHRONOS’s scalability, expressivity, and interpretability open new avenues in constrained edge computing, online control, computer vision, and beyond.

## 1 Introduction

Since Rosenblatt’s *perceptron* [1], *multilayer perceptrons* (MLPs) or *artificial neural networks* have come a long way in both data-driven and scientific modeling [2, 3, 4]. Many variations of neural networks have been proposed to achieve specific goals [5, 6, 7, 8]. However, at their core, most network architectures have remained the same; passing data through a set of activation functions, multiplying outputs by weights and biases to construct a non-linear mapping from input to output. Despite tremendous success, traditional neural architectures suffer from the curse of dimensionality: an exponential growth of trainable parameters for very high-dimensional and complex problems. This has helped lead to a six-order-of-magnitude increase in the cost of training from 2012 to 2018 [9]. In addition, interpretability and transferability remain a significant challenge for traditional neural networks.

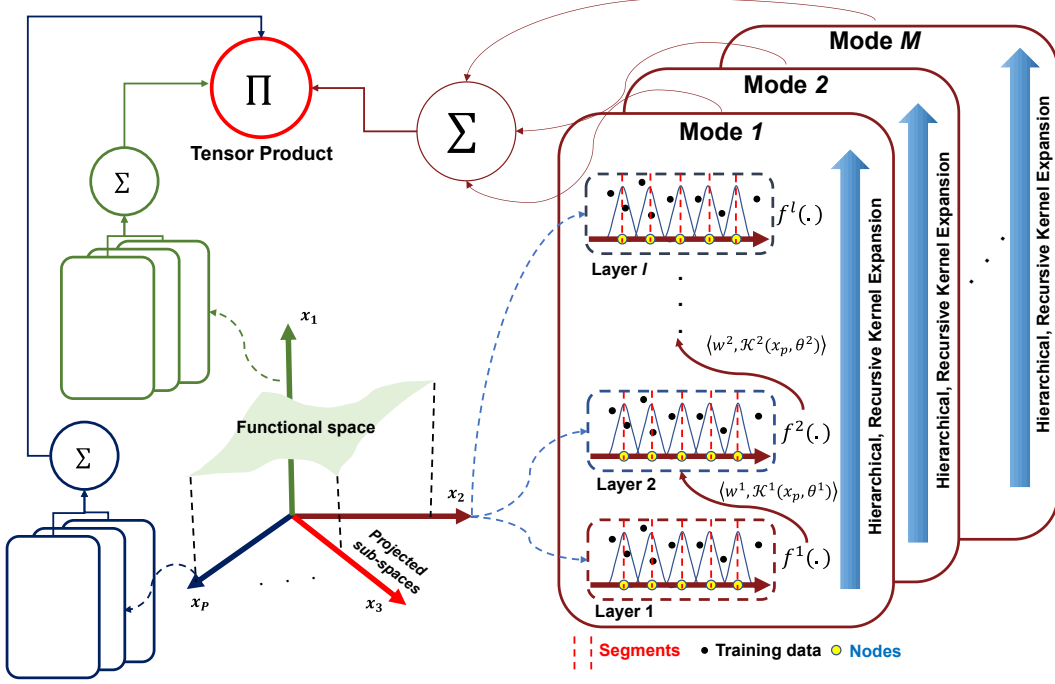


Figure 1: Schematic of KHRONOS’s architecture. Each input feature  $x_p$  is mapped via a kernel expansion (layers 1- $L$ ) defined on a small number of nodes (yellow) within each segment. Per-dimension feature vectors are projected by learned weights  $w$  and then combined via a tensor product ( $\Pi$ ) to form each mode. Finally,  $M$  such modes are summed ( $\Sigma$ ) to yield the surrogate.

Consequently, alternative network structures and activation functions have been explored, including kernel function-based non-parametric activations [10]. Some works have discussed, at length, the mathematics of kernel-based activation functions [11, 12, 13]. However, these works do not discuss how to reduce the size of the network while maintaining accuracy. Recently, the proposition of Kolmogorov-Arnold Neural Networks (KAN) provided a fresh perspective on neural architecture [14]. KANs embed basis functions, including kernel functions, into the data space instead of so-called neurons. KANs have shown impressive performance in many applications, demonstrating the promise of such alternative architectures [15, 14, 16]. Despite that, KANs still follow a collocation-based sampling method that leaves room for further reduction in structure and improvement in performance.

In this work, we introduce KHRONOS: an artificial intelligence framework tailored to the demands of modern computational science and engineering. KHRONOS is designed to operate across the full computing spectrum, from low-power edge devices in robots to exascale supercomputers. KHRONOS represents target fields as a hierarchical composition [17] of kernel expansions. In a single hidden layer network, this representation is effectively a Galerkin interpolation built with kernel shape functions, somewhat akin to an interpolating neural network (INN) [18]. In the subsequent sections, this article will discuss KHRONOS’s architecture and its application to three major classes of problems - *model-free*: in a pure data-driven environment, *model-based*: where there is a high-dimensional partial differential equation (PDE) to be solved, and *model-inverse*: where output-to-input mappings is needed from the forward mapping.

## 2 Methodology of KHRONOS

### 2.1 Architecture

Figure 1 illustrates KHRONOS’s core architecture. KHRONOS approximates a high-dimensional functional space by projecting onto one-dimensional feature subspaces. Each input feature space is partitioned into  $N_p^e$  segments, inducing a knot vector  $\{\theta_i\}_{i=1}^{N_p^e+1}$ . These knots are used to construct a finite set of kernels over the space. A key example used throughout this work is that of second-order

(quadratic) B-spline kernels [19]. These are defined over four consecutive knots and are compactly supported on the three inscribed segments. By extending the knot vector by two points beyond the domain at each end (bringing us to  $N_p^e + 5$  total knots/nodes), one obtains  $N_p^k = N_p^e + 2$  quadratic B-spline basis functions on the domain which satisfy partition-of-unity.

These kernel evaluations are linearly combined via learnable weights into a local feature approximation within each one-dimensional subspace. Each such projection constitutes a single layer, with multiple layers stacked by sending the output of a previous projection as an input into the next. This can be seen as analogous to the successive feature maps in a convolutional neural network (CNN) [5]. Unlike standard networks, however, nonlinearity is inherent to the choice of kernel basis rather than imposed by external activation functions. Each of these one-dimensional feature maps is a mode contribution, with a single mode assembled by their overall product. Several such modes, each with their own learned feature spaces, are then superposed to produce the surrogate output.

## 2.2 Mathematical Formulation

### 2.2.1 Model Ansatz and Forward Propagation

KHRONOS aims to find a representation  $\hat{u}(x)$  for a target field  $u(x)$  over a  $P$ -dimensional input feature  $x = (x_1, \dots, x_p, \dots, x_P)$ . It does this by hierarchically composing per-feature kernel expansions into full-parameter modes. Each feature  $x_p$  is first mapped through a sequence of  $L$  expansion layers. The feature map of the  $l$ -th layer for parameter  $p$  is denoted,

$$f_p^{(l)} = \mathcal{K}(f_p^{(l-1)}, \theta_p^{(l)}), \quad (1)$$

where  $\theta_{p,i}^{(l)}$  are the kernel's parameters,  $f_{p,i}^{(0)}(x_p) = x_p$ , and  $f_p^{(l-1)} \equiv f_p^{(l-1)}(x_p)$  is the scalar output from the previous expansion layer. Each layer's output is formed by a weighted sum of these kernels,

$$f_p^{(l)}(x_p) = \sum_{i=1}^{N_{p,l}} w_{p,i}^{(l)} \mathcal{K}(f_p^{(l-1)}(x_p), \theta_{p,i}^{(l)}), \quad (2)$$

$$= \sum_{i=1}^{N_{p,l}} w_{p,i}^{(l)} f_{p,i}^{(l)}, \quad (3)$$

$$= \langle w_p^{(l)}, f_p^{(l)} \rangle. \quad (4)$$

After  $L$  such compositions, each feature  $p$  yields a scalar  $f_p^{(L)}(x_p)$ . KHRONOS then builds a number of separable modes  $M_j(x)$ , each learning its own feature-wise layer outputs,  $f_{p,j}^{(L)}(x_p)$ . Modes are constructed by multiplying across features,

$$M_j(x) = \prod_{p=1}^P f_{p,j}^{(L)}(x_p). \quad (5)$$

There are two approaches to training modes,

1. Cooperative (joint) learning. The number of modes is predefined as  $J$ . KHRONOS initializes each with separate parameters and superposes them,

$$\hat{u}(x) = \sum_{j=1}^J M_j(x). \quad (6)$$

This superposition is trained in its entirety, with modes thus being trained concurrently.

2. Sequential learning. A single mode  $M_1(x)$  is initialized and trained. The next mode then seeks to represent the new target field,  $u_1(x) = u(x) - M_1(x)$ . This is iterated until an acceptable tolerance  $\epsilon$  is met, so that the number of modes is  $J_{tol} = \min\{j : \|u - \sum_{i=1}^j M_i\| < \epsilon\}$ . The surrogate is again the superposition of all of these modes,

$$\hat{u}(x) = \sum_{j=1}^{J_{tol}} M_j(x). \quad (7)$$

## 2.2.2 Loss Functions

**Model-Free** A model-free (or supervised learning) approach involves learning from labeled data. KHRONOS, in particular, learns from data structured as  $d$ -input, scalar-output pairs  $\{(x_i, u_i)\}_{i=1}^I$ ,  $x_i \in \mathbb{R}^d$ ,  $u_i \in \mathbb{R}$ . Then for a parametric model  $\hat{u}(x; \theta)$ ,  $\theta$  the model parameters, the model-free, mean-squared error loss is given by

$$L_{mse} = \frac{1}{I} \sum_{i=1}^I (\hat{u}(x_i; \theta) - u_i)^2. \quad (8)$$

**Model-Based** For physics-based training (solving), the loss function for a space-time-parameter can be constructed in two ways: a) using collocation-based method akin to PINNs [8], or b) using Galerkin-like weak formulation. The space-time-parameter is defined over  $x \in \Omega$ , enclosed by a boundary  $\partial\Omega$ , with time  $t \in [0, T]$ , and parameters  $d_1, \dots, d_p \in \mathcal{P} \subset \mathbb{R}^p$ . Given a second order spatial differential operator  $\mathcal{L}$ , first-order boundary differential operator  $\mathcal{B}$ , source term  $f(x, t; d)$  and boundary source term  $g(x, t; d)$  the target PDE is defined

$$\partial_t u - \mathcal{L}u = f \quad \text{in } \Omega, \quad (9)$$

$$\mathcal{B}u = g \quad \text{on } \partial\Omega, \quad (10)$$

$$u = u_0 \quad \text{at } t = 0. \quad (11)$$

For a neural surrogate  $\hat{u}(x, t, d; \theta)$ , with *network* parameters  $\theta$ , residuals are then defined,

$$r_\Omega = \partial_t \hat{u} - \mathcal{L}\hat{u} - f, \quad (12)$$

$$r_{\partial\Omega} = -\mathcal{B}\hat{u} - g. \quad (13)$$

With given hyperparameters  $\alpha_\Omega, \alpha_{\partial\Omega}$ , and residuals defined in 12 a strong formulation loss function can then be constructed,

$$L_{strong}(\theta) = \frac{\alpha_\Omega}{N_\Omega} \sum_{k,n,l} r_\Omega(x_k, t_n, d_l; \theta)^2 + \frac{\alpha_{\partial\Omega}}{N_{\partial\Omega}} \sum_{b,n,l} r_{\partial\Omega}(x_b, t_n, d_l; \theta)^2, \quad (14)$$

where  $\{x_k\}_{k=1}^{N_\Omega} \subset \Omega$ ,  $\{x_b\}_{b=1}^{N_{\partial\Omega}} \subset \partial\Omega$ ,  $\{t_n\}_{n=1}^{N_t} \subset [0, T]$  and  $\{d_l\}_{l=1}^{N_d} \subset \mathcal{P}$ . This is a collocation loss, evaluated at  $N_\Omega$  interior points and  $N_{\partial\Omega}$  boundary points. Collocation based approaches can face sensitivity issues, where careful sampling is required to avoid spiky errors between points. Further, the surrogate is required to be sufficiently smooth in order for  $\mathcal{L}u$  to be well defined at collocation points.

A Galerkin weak formulation has less stringent smoothness requirements. Namely, the spatial requirement is  $\hat{u}(\cdot, t, d) \in H^1(\Omega)$ ,  $\forall t \in [0, T]$ . Then, the bilinear form  $a(\hat{u}, v) = \int_\Omega a \nabla \hat{u} \cdot \nabla v dx$  is well defined  $\forall v \in H^1(\Omega)$ . The temporal requirement is that for almost every  $x \in \Omega$  and  $d \in \mathcal{P}$ ,  $\hat{u}(x, \cdot, d) \in L^2(0, T)$ . Thus, the choice of second-order splines (or any kernel in  $H^1(\Omega) \times L^2(0, T)$ ) guarantees existence and uniqueness of solutions for a sufficiently regular and coercive operator  $\mathcal{L}$ .

The weak formulation of (9) is defined

$$\int_0^T \int_\Omega \partial_t u v \, dx \, dt - \int_0^T \int_\Omega v \mathcal{L}u \, dx \, dt = \int_0^T \int_\Omega f v \, dx \, dt, \forall v \in V(\Omega) \times L^2(0, T), \quad (15)$$

with test space  $V \subseteq H^1(\Omega)$  depending on the boundary conditions. Given a test function  $\hat{u} \in H^1(\Omega) \times L^2(0, 1)$ , the associated weak residual is defined as,

$$\mathcal{R}\{\hat{u}, v\} = \int_0^T \int_\Omega v \partial_t \hat{u} - v \mathcal{L}\hat{u} - f v \, dx \, dt, \forall v \in V(\Omega) \times L^2(0, T). \quad (16)$$

For training, a weak residual loss is then defined as,

$$L_{weak}(\theta) = \sum_j (\mathcal{R}\{\hat{u}, v_j\})^2, \quad (17)$$

for a finite set of test functions  $\{v_j\} \subset V(\Omega) \times L^2(0, T)$ . Or for a collocation-based loss,

$$L_{weak}(\theta) = \int_0^T \int_\Omega (\partial_t \hat{u} - \mathcal{L}\hat{u} - f)^2 v^2 \, dx \, dt, \quad (18)$$

with a fixed choice for  $v$  - typically  $v \equiv 1$ .

For a linear, symmetric, and coercive  $\mathcal{L}$  -such as the Laplacian  $-\Delta$  used as an example in Section 3.2 - we may equivalently minimize an energy-based loss.

**Mixed Models** In practice, it is possible to construct a loss function as a combination of model-free and model-based terms. A common choice is to take  $\alpha_{data}$ ,  $\alpha_{model}$ , and write,

$$L_{mixed}(\theta) = \alpha_{data}L_{mse}(\theta) + \alpha_{model}L_{weak}(\theta). \quad (19)$$

Such a formulation is useful in settings with limited data and uncertain or partially known physics, or when an empirical-model balance is required.

### 2.2.3 Inverse Modeling

Inverse modeling is the task of inferring unknown parameters from observed outputs, in particular from a learned model. Formally, let  $\hat{u} : \mathcal{X} \rightarrow \mathcal{Y}$  be a learned KHRONOS surrogate that maps inputs  $x \in \mathcal{X}$  to outputs  $\hat{u} \in \mathcal{Y}$ . Given some observed outcome  $z \in \mathcal{Y}$ , an inverse modeling problem seeks an input  $\alpha \in \mathcal{X}$  so that,

$$\hat{u}(\alpha) = z. \quad (20)$$

With the right choice of kernel, KHRONOS's constructs a continuously differentiable  $\hat{u}$ . This allows for gradient-based root-finding or optimization algorithms. One choice investigated in Section 3.3 is Gauss-Newton [20]. If  $x_k$  is the  $k$ -th Gauss-Newton iteration, the next iterate  $x_{k+1}$  is found by

$$x_{k+1} = x_k - \frac{\hat{u} - z}{|\nabla \hat{u}|^2} \nabla \hat{u}, \quad (21)$$

with  $x_0 \in \mathcal{X}$  an initial guess.

Gauss-Newton is lightweight, requiring a single forward and gradient evaluation in one update with automatic differentiation. Further, it is *embarrassingly parallel* across different guesses  $x_0$ , and different targets  $z$ . This makes it a strong candidate for *batch inversion*; parallel evaluation of initial conditions sampled over  $\mathcal{X}$ . This allows for entire level set recovery on the order of single milliseconds. This performance brings inverse modeling into real-time, online and high-throughput regimes from what is traditionally an offline process.

## 3 Performance Analysis of KHRONOS

### 3.1 Model-Free

To assess model-free, supervised performance, KHRONOS is compared to some high-performing contemporary models: Random Forest (RF), XGBoost and a multilayer perceptron (MLP). The toy problem is the 8-dimensional borehole function,

$$u(p) = 2\pi p_3(p_4 - p_6) \left( \log \left( \frac{p_2}{p_1} \right) \left( 1 + 2 \frac{p_7 p_3}{\log \left( \frac{p_2}{p_1} \right) p_1^2 p_8} + \frac{p_3}{p_5} \right) \right)^{-1}, \quad (22)$$

$$(23)$$

with features,

$$\text{Borehole radius (m): } p_1 \in [0.05, 0.15], \quad (24)$$

$$\text{Radius of influence (m): } p_2 \in [100, 50000], \quad (25)$$

$$\text{Transmissivity of upper aquifer (m}^2\text{/yr): } p_3 \in [63700, 115600], \quad (26)$$

$$\text{Potentiometric head of upper aquifer (m): } p_4 \in [990, 1110], \quad (27)$$

$$\text{Transmissivity of lower aquifer (m}^2\text{/yr): } p_5 \in [63.1, 116], \quad (28)$$

$$\text{Potentiometric head of lower aquifer (m): } p_6 \in [700, 820], \quad (29)$$

$$\text{Length of borehole (m): } p_7 \in [1120, 1680], \quad (30)$$

$$\text{Hydraulic conductivity of borehole (m/yr): } p_8 \in [9855, 12045]. \quad (31)$$

This function is typical for testing uncertainty quantification and surrogate models. Data, in the form of input-output pairs, is generated by sampling the equation at 100,000 points using Latin Hypercube sampling. This data is normalized, and then split 70/30, train-test. Table 1 shows the performance of

Table 1: Benchmark comparison of surrogate models on the borehole problem (22), sampled at 100,000 points with a 70/30 train-test split. RF used 100 estimators with a maximum depth of 15, XGBoost had 200 estimators with a max depth of 8, the MLP had 2 hidden layers with widths of 50, and KHRONOS was run with 4 kernels per-dimension and 3 modes.

Metric	Random Forest[21]	XGBoost [22]	MLP	KHRONOS
Trainable parameters	4,261,376	84,600	5601	240
Training time (s)	2.8	1.5	22	0.87
Inference time (ms)	75	61	0.7	0.2
Test MSE	$1.0 \times 10^{-4}$	$3.3 \times 10^{-5}$	$2.8 \times 10^{-5}$	$2.2 \times 10^{-5}$
Test $R^2$	0.9969	0.9990	0.9992	0.9998

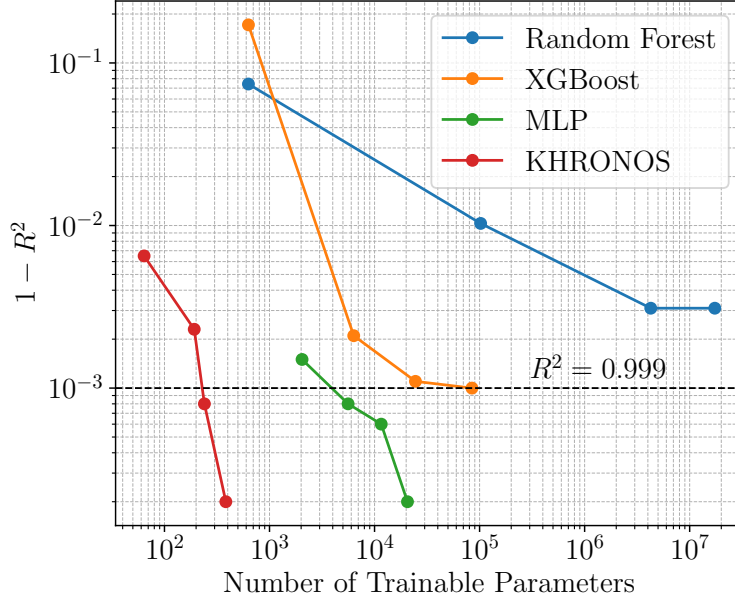


Figure 2: Plot of convergence toward perfect accuracy,  $1 - R^2 \rightarrow 0$ , as trainable parameters increase for each surrogate model

each models. To provide a consistent saturation point, baseline model complexity (number of trees, maximum depth, number and width of layers) was increased until the model achieved a validation ( $R^2$ ) score of at least 0.999. This parameter saturation is shown in figure 2.

RF was unable to achieve the target  $R^2$ -score, saturating at 0.9969. Remarkably, KHRONOS achieved an  $R^2$ -score of 0.9935 with as few as 64 trainable parameters. Furthermore, it was the only tested surrogate able to hit the target  $R^2$  in under a second. In addition to its low parameter count, this efficiently comes from its computational structure. Whereas MLPs require dense matrix operations of complexity  $O(n_{layers} \cdot n_{widths} \cdot n_{widths})$ , the dominant cost in KHRONOS is  $O(n_{modes} \cdot n_{dim})$  in mode construction. For the borehole problem, this is  $O(1)O(10)O(10)$  for an MLP but only  $O(1)O(10)$  for KHRONOS.

### 3.2 Model-Based

In this section,  $L_2^2$  denotes the squared  $L_2$ -norm over  $\Omega = [0, 1]^2$ ,  $\|u\|_{L_2(\Omega)}$ , and  $H_1^2$  denotes the squared  $H^1$ -seminorm  $\|\nabla u\|_{L_2(\Omega)}^2$ . KHRONOS is used as a model-based solver, with a canonical

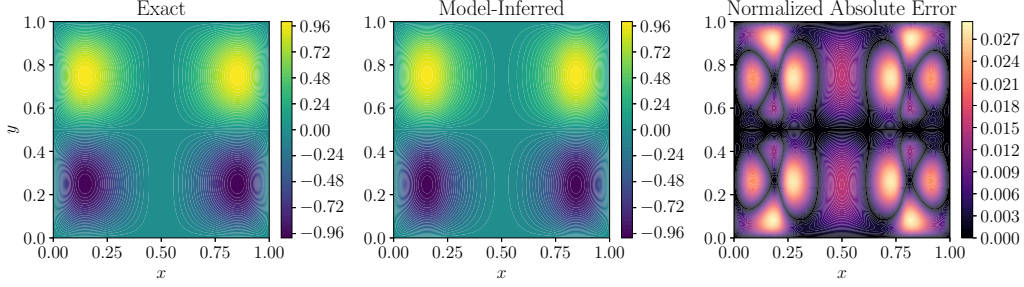


Figure 3: Exact solution, model prediction and the normalized absolute error for a 16-parameter KHROS solve

2D Poisson problem taken as example [23],

$$-\Delta u = f \quad \text{in } \Omega, \quad (32)$$

$$u = 0 \quad \text{on } \partial\Omega, \quad (33)$$

with  $\Omega = [-1, 1]^2$ ,  $f(x, y) = \pi^2(1 + 4y^2) \sin(\pi x) \sin(\pi y^2) - 2\pi \sin(\pi x) \cos(\pi y^2)$ . This system is transformed by  $(\tilde{x}, \tilde{y}) = 2(x, y) - 1$ , so that  $\tilde{\Omega} = [0, 1]^2$ ,  $\tilde{f}(\tilde{x}, \tilde{y}) = 4f(x, y)$ , admitted the same solution  $u(\tilde{x}, \tilde{y})$ . Equation (32) admits exact solution  $u(x, y) = \sin(\pi x) \sin(\pi y^2)$ . The corresponding energy functional is defined

$$\varepsilon(\tilde{u}) = \int_0^1 \int_0^1 \left( \frac{1}{2} |\nabla \tilde{u}|^2 - \tilde{f} \tilde{u} \right) d\tilde{x} d\tilde{y}, \quad (34)$$

and admits a unique minimizer in  $H_0^1(\Omega)$ , under standard assumptions on  $f \in L^2(\Omega)$ . This follows from the Direct Method in the calculus of variations [24]. KHROS constructs a kernel-based approximation  $\hat{u}(\tilde{x}, \tilde{y})$  using second-order B-splines. This choice of kernel ensures  $\hat{u}(\tilde{x}, \tilde{y}; \theta) \in H_0^1(\Omega)$  and is thus admissible in the variational formulation. It can therefore be trained by minimizing  $L(\theta) = \varepsilon(\hat{u}(\tilde{x}, \tilde{y}; \theta))$ . In this case, KHROS is then, in effect, meshfree, variationally consistent and free of costly matrix operations. Figure 3 shows an example of a hyper-light 16-parameter KHROS solve.

Table 2 summarizes KHROS’s performance over a range of degrees of freedom (DoFs). Figure 4 demonstrates the linear increase in training time per epoch with increasing DoF, as well as shows log-log plots of errors in the square  $L_2$ -norm and square  $H_1$ -seminorm. The  $L_2^2$  and  $H_1^2$  errors exhibit empirical scaling laws of  $\text{DoF}^{-4}$  and  $\text{DoF}^{-3}$ , respectively, the same as KAN [23] constructed with second order b-splines. While both architectures exhibit similar empirical scaling, KHROS enjoys a substantial head start. Whereas KAN requires 150 trainable parameters to drive the  $L_2^2$  error down to  $10^{-6}$ , KHROS attains  $L_2^2 \sim 10^{-8}$ , on the same parameter budget - a near hundredfold increase in accuracy.

Table 2: Performance of KHROS on the 2D Poisson equation using energy minimization and trapezoidal quadrature, run for a fixed 10000 epochs per resolution.

DoF	Epoch Time (ms)	Inference ( $\mu\text{s}$ )	$L_2^2$	$H_1^2$
16	0.7	270	$4.7 \times 10^{-4}$	$2.4 \times 10^{-1}$
32	0.7	240	$7.0 \times 10^{-6}$	$1.8 \times 10^{-2}$
64	0.6	230	$2.6 \times 10^{-6}$	$7.7 \times 10^{-3}$
128	0.9	330	$3.7 \times 10^{-8}$	$5.7 \times 10^{-4}$
256	1.4	380	$2.3 \times 10^{-9}$	$9.2 \times 10^{-5}$
512	2.3	460	$5.5 \times 10^{-10}$	$2.8 \times 10^{-5}$

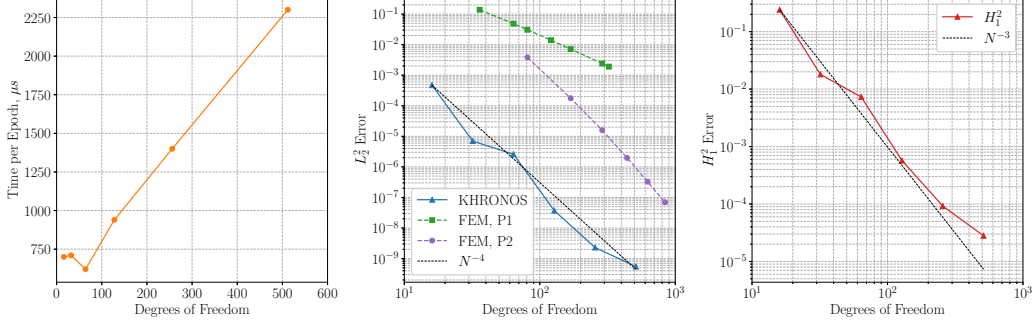


Figure 4: Plot showing time per epoch ( $\mu s$ ),  $L_2^2$  error and  $H_1^2$  error as parameters increase. The second plot also shows the  $L_2^2$  errors incurred by P1 and P2 Lagrange element FEM.  $N^{-4}$  and  $N^{-3}$  scaling laws for  $L_2^2$  and  $H_1^2$  errors, respectively, are shown for reference

Table 3: Batched Newton-inversion on an A100. Total elapsed time, per-point latency, failure rate (points with residual  $>1e-3$ ), and residual

Batchsize	Total Time (ms)	Time per Point ( $\mu s$ )	Failure Rate %	RMSE
500	4.9	9.7	0.2	$1.2 \times 10^{-3}$
1000	5.3	5.3	0.3	$1.2 \times 10^{-3}$
2000	5.1	2.6	0.3	$1.2 \times 10^{-3}$
4000	6.2	1.5	0.1	$1.2 \times 10^{-3}$
8000	5.9	0.7	0.3	$1.2 \times 10^{-3}$
16000	6.9	0.4	0.3	$1.2 \times 10^{-3}$

### 3.3 Model Inversion

In this section, the continuously differentiable surrogate found by KHRONOS is exploited in order to perform batch model inversion. This is highlighted by the toy problem,

$$u(x, y) = \sin(4\pi x) \sin(2\pi y) + \frac{1}{2} \sin(6\pi x) \sin(3\pi y), \quad (35)$$

on  $[0, 1]^2$ . KHRONOS is first trained on generated by Latin Hypercube sampling at  $n$  points,  $n = 500, 1000, 2000, 4000, 8000$  and  $16000$ . The goal is then inversion to find the level set  $\hat{u} = 0$ , via Gauss-Newton for 10 iterations. Table 3 reports total latency, per-point latency, convergence failure rate, and RMSE for each batch. As the GPU is saturated with sufficient batch size increases, sub-microsecond per-point inversion times are seen. Failure rates and errors remain steady across the tested batch sizes, highlighting the strength of this divide-and-conquer approach, even in a highly non-convex example.

## 4 Conclusions

This work has presented KHRONOS, a separable, kernel-based surrogate architecture that unifies model-free, model-based and model-inverse learning. Empirical results demonstrated that KHRONOS:

- **Model-free:** outperforms Random Forest, XGBoost and multilayer perceptron baselines with reduced training times - the only model to achieve a target  $R^2$ -score in under a second - and one to four orders of magnitude fewer parameters on the 8D borehole benchmark. Furthermore, it achieves  $R^2 > 0.99$  with a remarkably low number of trainable parameters: 64.
- **Model-based:** achieves  $L_2^2$  DoF $^{-4}$  and  $H_1^2$  DoF $^{-3}$  scaling on a 2D Poisson benchmark, slashing the number of trainable parameters compared to FEM, MLPs and KANs while



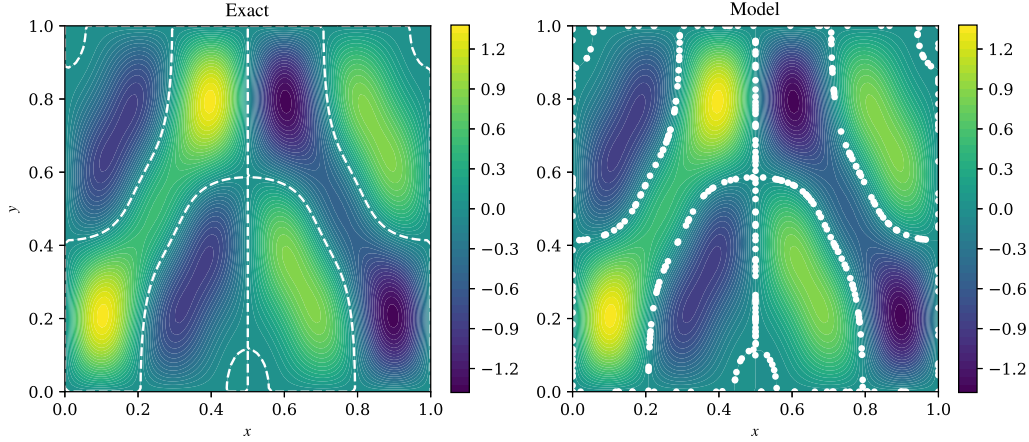


Figure 5: Batch inversion, 400 points, of KHRONOS on a highly non-convex toy example

demonstrating lower  $L_2^2$  and  $H_1^2$  errors, as well as a linear increase in runtime with degrees of freedom.

- **Model-inverse:** enables batched Gauss-Newton inversion for highly nonconvex targets at sub-microsecond-per-sample latency, with robust convergence across thousands of initializations.

## 5 Limitations

The current model-based solver uses collocation-based finite-difference/trapezoidal integration over a dense grid rather than a per-coordinate Gauss-Legendre quadrature and automatic differentiation scheme. Calculating the energy functional  $\varepsilon(\hat{u})$  using a dedicated integration routine of this nature would reduce the loss evaluation cost - by far the greatest bottleneck - by  $10^2 - 10^4\times$ . Further, KHRONOS's current implementation assumes a regular grid over  $[0, 1]^d$ , thus cannot yet handle unstructured meshes or non-rectangular geometries.

As a novel architecture, KHRONOS has only been tested on a handful of benchmark problems. Its behavior on complex, multidimensional PDEs and inversion remains unverified. Moreover, it lacks pre- and post-processing utilities, as well as community-vetted best practices.

## 6 Future Work

KHRONOS can potentially be extended and applied in many fields of science and engineering, including online monitoring and control of additive manufacturing, inverse design of microstructure, multiscale computation of hierarchical materials systems, and computer vision algorithms for autonomous robotics. Being a kernel-based method, it is natural to apply KHRONOS to image-based problems. Thus far, KHRONOS has shown promise in efficiently learning differentiable image representations - potentially useful for visual servoing.

In solving the issue of separable integration, one approach is to fit a separable KHRONOS surrogate to the source term, enabling separable integration. Work here is ongoing. Finally, more extensive testing against contemporary architectures is required to verify all of KHRONOS's potential claims.

## References

- [1] Frank Rosenblatt. The perceptron: a probabilistic model for information storage and organization in the brain. *Psychological review*, 65(6):386, 1958.
- [2] Michael I Jordan and Tom M Mitchell. Machine learning: Trends, perspectives, and prospects. *Science*, 349(6245):255–260, 2015.

- [3] Salvatore Cuomo, Vincenzo Schiano Di Cola, Fabio Giampaolo, Gianluigi Rozza, Maziar Raissi, and Francesco Piccialli. Scientific machine learning through physics-informed neural networks: Where we are and what's next. *Journal of Scientific Computing*, 92(3):88, 2022.
- [4] Steven L Brunton and J Nathan Kutz. Promising directions of machine learning for partial differential equations. *Nature Computational Science*, 4(7):483–494, 2024.
- [5] Yann LeCun, Bernhard Boser, John S Denker, Donnie Henderson, Richard E Howard, Wayne Hubbard, and Lawrence D Jackel. Backpropagation applied to handwritten zip code recognition. *Neural computation*, 1(4):541–551, 1989.
- [6] David E Rumelhart, Geoffrey E Hinton, Ronald J Williams, et al. Learning internal representations by error propagation, 1985.
- [7] Ashish Vaswani, Noam Shazeer, Niki Parmar, Jakob Uszkoreit, Llion Jones, Aidan N Gomez, Łukasz Kaiser, and Illia Polosukhin. Attention is all you need. *Advances in neural information processing systems*, 30, 2017.
- [8] Maziar Raissi, Paris Perdikaris, and George E Karniadakis. Physics-informed neural networks: A deep learning framework for solving forward and inverse problems involving nonlinear partial differential equations. *Journal of Computational physics*, 378:686–707, 2019.
- [9] Roy Schwartz, Jesse Dodge, Noah A Smith, and Oren Etzioni. Green ai. *Communications of the ACM*, 63(12):54–63, 2020.
- [10] Simone Scardapane, Steven Van Vaerenbergh, Simone Totaro, and Aurelio Uncini. Kafnets: Kernel-based non-parametric activation functions for neural networks. *Neural Networks*, 110:19–32, 2019.
- [11] Po-Sen Huang, Haim Avron, Tara N Sainath, Vikas Sindhwani, and Bhuvana Ramabhadran. Kernel methods match deep neural networks on timit. In *2014 IEEE international conference on acoustics, speech and signal processing (ICASSP)*, pages 205–209. IEEE, 2014.
- [12] Behrooz Ghorbani, Song Mei, Theodor Misiakiewicz, and Andrea Montanari. When do neural networks outperform kernel methods? *Advances in Neural Information Processing Systems*, 33:14820–14830, 2020.
- [13] Mariia Seleznova and Gitta Kutyniok. Neural tangent kernel beyond the infinite-width limit: Effects of depth and initialization. In *International Conference on Machine Learning*, pages 19522–19560. PMLR, 2022.
- [14] Ziming Liu, Pingchuan Ma, Yixuan Wang, Wojciech Matusik, and Max Tegmark. Kan 2.0: Kolmogorov-arnold networks meet science. *arXiv preprint arXiv:2408.10205*, 2024.
- [15] Nisal Ranasinghe, Yu Xia, Sachith Seneviratne, and Saman Halgamuge. Ginn-kan: Interpretability pipelining with applications in physics informed neural networks. *arXiv preprint arXiv:2408.14780*, 2024.
- [16] Prakash Thakolkaran, Yaqi Guo, Shivam Saini, Mathias Peirlinck, Benjamin Alheit, and Siddhant Kumar. Can kan cans? input-convex kolmogorov-arnold networks (kans) as hyperelastic constitutive artificial neural networks (cans). *arXiv preprint arXiv:2503.05617*, 2025.
- [17] Sourav Saha, Zhengtao Gan, Lin Cheng, Jiaying Gao, Orion L Kafka, Xiaoyu Xie, Hengyang Li, Mahsa Tajdari, H Alicia Kim, and Wing Kam Liu. Hierarchical deep learning neural network (hidenn): an artificial intelligence (ai) framework for computational science and engineering. *Computer Methods in Applied Mechanics and Engineering*, 373:113452, 2021.
- [18] Chanwook Park, Sourav Saha, Jiachen Guo, Hantao Zhang, Xiaoyu Xie, Miguel A. Bessa, Dong Qian, Wei Chen, Gregory J. Wagner, Jian Cao, and Wing Kam Liu. Interpolating neural network: A novel unification of machine learning and interpolation theory. *arXiv preprint, arXiv:2404.10296*, 2024.
- [19] Les Piegl and Wayne Tiller. *The NURBS Book*. Springer, 2nd edition, 1997.

- [20] Roger Fletcher. *Practical methods of optimization*. John Wiley & Sons, 2000.
- [21] Leo Breiman. Random forests. *Machine learning*, 45:5–32, 2001.
- [22] Tianqi Chen and Carlos Guestrin. Xgboost: A scalable tree boosting system. In *Proceedings of the 22nd acm sigkdd international conference on knowledge discovery and data mining*, pages 785–794, 2016.
- [23] Ziming Liu, Yixuan Wang, Sachin Vaidya, Fabian Ruehle, James Halverson, Thomas Y. Hou, Marin Soljačić, and Max Tegmark. Kolmogorov–arnold networks (kan). *Preprint*, 2024. arXiv:2404.19756.
- [24] Enrico Giusti. *Direct methods in the calculus of variations*. World Scientific, 2003.